INT. J. NUM. METH. HEAT FLUID FLOW, VOL. 5, 423–443 (1995)

NUMERICAL EXPERIMENTS ON LAMINAR NATURAL CONVECTION IN RECTANGULAR CAVITIES WITH AND WITHOUT HONEYCOMB-STRUCTURES

H. SCHWEIGER, A. OLIVA, M. COSTA, C. D. PÉREZ SEGARRA AND A. IVANČIĆ

Laboratori de Termotècnia i Energètica, Departament de Màquines i Motors Tèrmics, Universitat Politècnica de Catalunya, C/Colom 9, E-08222 Terrassa, Barcelona, Spain

ABSTRACT

Two-dimensional finite difference calculations are carried out to study laminar flow in longitudinal and transverse convection rolls for three different geometries: a single rectangular cavity with high aspect ratio; a double cavity with a thin separation sheet; and a double cavity with a separation sheet and a honeycomb structure. The equations for the convection-diffusion in the fluid and conduction in the solid region are solved simultaneously. Good agreement with experimental data is achieved for Rayleigh numbers not too high above the critical value for the onset of secondary convection rolls ($Ra < 8500$ for vertical and $Ra < 2700$ for horizontal cavities filled with air). Simulation fails for inclined cavities, where the flow structure is essentially three-dimensional.

KEY WORDS Natural convection Inclined cavities Secondary flow Convection suppression Honeycombs Segregated method

NOMENCLATURE

$A = L_x/L_z$	cavity aspect ratio		Navier Stokes equation (10)
$A_1 = L_x/L_1$	aspect ratio of an individual cavity	k_b	thermal conductivity of the separation sheet and honeycomb
$A_c = L_c/L_1$	aspect ratio of a honeycomb cell	k_c	wavenumber of the convection cells (non-dimensional)
$A_{grid} = \Delta x/\Delta z$	grid aspect ratio	k_{cr}	critical wavenumber (non-dimensional)
$B = L_2/L_1$	ratio of the z-dimensions of upper and lower cavity	L_x, L_y, L_z	dimension of the cavity in x,y,z-direction
g	gravitation constant (dimensional)	$L = L_z$	characteristic length
g	gravitation vector (non-dimensional)	L_1, L_2	spacing of the two halfs of a double cavity
g_x, g_y, g_z	x,y,z-component of the gravitation vector (non-dimensional)	L_b	thickness of the separation sheet and honeycomb cell walls
k	thermal conductivity of the fluid	L_c	x-dimension of the honeycomb cells
K	constant for the additional term in the		

0961–5539/95/050423–21$2.00

Received July 1993
Revised March 1994

N_c	number of convection cells
N_x, N_z	number of control volumes in x,z-direction
$Nu = \dfrac{\dot{q} \cdot L}{k \cdot \Delta\theta}$	Nusselt number
p	pressure
$\tilde{p} = (p/\rho - \mathbf{r} \cdot \mathbf{g})/v_0^2$	nondimensional pressure
$Pr = \nu/\alpha$	Prandtl number
$\dot{q}$	average heat flux through the isothermal boundaries
$\dot{q}_i$	heat flux at the solid-fluid interface
R	heating rate (non-dimensional)
$\mathbf{r} = (x,y,z)$	vector to a point in the three dimensional space (non-dimensional)
$Ra = \dfrac{\rho\beta g \Delta\theta L^3}{\nu \cdot \alpha}$	Rayleigh number
$Ra_1 = \dfrac{\rho\beta g \Delta\theta_1 L_1^3}{\nu \cdot \alpha}$	Rayleigh number based on L_1 and $\Delta\theta_1$
Ra_{cr}	critical Rayleigh number for the onset of secondary flow
Ra_{osc}	critical Rayleigh number for the onset of periodic time-dependent motion
$T = (\theta - \theta_m)/\Delta\theta$	non-dimensional temperature
T_s	temperature at a grid point in the solid region
T_f	temperature at a grid point in the fluid region
$\Delta T = 1$	non-dimensional temperature difference between the isothermal sidewalls
t	time (non-dimensional)
Δt	iterative time step (non-dimensional)
$t_0 = L/v_0$	characteristic time
t_1	final time of measurements (non-dimensional)
t_{CPU}	computation time in minutes
u,v,w	x,y,z-components of the velocity vector (non-dimensional)
$\mathbf{v}$	velocity vector (non-dimensional)
v_0	characteristic velocity
$\Delta x, \Delta y, \Delta z$	size of control volumes (non-dimensional)
Δx_{if}	distance between fluid grid point and solid-fluid interface
Δx_{si}	distance between solid grid point and solid-fluid interface
x,y,z	nondimensional coordinates (characteristic length L)
$\mathbf{y}$	unity vector in y-direction
α	inclination angle between x-axis and horizontal plane, thermal diffusivity of the fluid
$\alpha_{fluid}, \alpha_{solid}$	thermal diffusivities of fluid and solid elements
$\tilde{\alpha}$	non-dimensional thermal diffusivity
β	inclination angle between y-axis and horizontal plane, thermal expansion coefficient of the fluid
ε	convergence criterion for mass production
λ_c	wavelength of convection cells (non-dimensional)
$\lambda_{cr} = 2\pi/k_{cr}$	critical wavelength (non-dimensional)
ν	kinematic viscosity
θ	temperature
θ_c, θ_h	temperatures of the cold and hot boundary plane
$\theta_m = (\theta_h + \theta_c)/2$	mean temperature of the cavity
$\Delta\theta = \theta_h - \theta_c$	temperature difference between the isothermal sidewalls
$\Delta\theta_1 = \dfrac{\Delta\theta L_1}{L_1 + L_b k/k_b + L_2}$	temperature difference over the half cavity with spacing L_1 for pure conduction
ρ	fluid density
τ_{osc}	period time of oscillations (non-dimensional)
ψ'	stream function of the perturbation velocity field (non-dimensional)
$\hat{\psi}$	amplitude of the

perturbation stream function (non-dimensional)	ψ_{max}	the stream function (non-dimensional) maximum value of the stream function (non-dimensional)
peak to peak value of the periodic part of		

INTRODUCTION

A great variety of theoretical and experimental work has been undertaken to study natural convection in rectangular enclosures, since it is important in a wide range of technical applications, for example in window glazing, solar collectors and in the cooling of electronic equipment.

Most of the theoretical work has been carried out for a differentially heated cavity with an infinite aspect ratio. For this infinite cavity, an analytical solution of the governing equations exists in the form of a parallel shear flow with a cubic velocity profile and a linear temperature gradient between the isothermal plates[1].

At a critical Rayleigh number (Ra_{cr}) this base shear flow becomes unstable. For near vertical cavities filled with air ($Pr = 0.71$) the resulting flow pattern consists of transversal convection rolls, with a critical Rayleigh number $Ra_{cr} = 5700$ and a critical wavenumber $k_{cr} = 2.81$ at the inclination angle $\alpha = 90°$. The wavenumber of the flow pattern decreases with increasing Ra. Linear stability analysis of the roll patterns shows that already at sightly supercritical values of $Ra \approx 6070$ ($1.06\, Ra_{cr}$) more complex three-dimensional flow patterns occur, and at values of Ra as low as 6200 ($1.09\, Ra_{cr}$) the flow becomes periodically time-dependent[2].

For inclination angles between 0° and 70°, longitudinal convection rolls are more stable[3,4]. The critical value of the Rayleigh number for longitudinal rolls is $Ra_{cr} = 1708/\cos\alpha$, with a critical wavenumber $k_{cr} = 3.117$. Stability analysis of longitudinal rolls[5], shows a transition to a three-dimensional wavy flow pattern, for inclination angles between 10° and 70°, already appear at $Ra - Ra_{cr} = 10$.

Linthorst *et al.*[6] have, from a visualization of the secondary flow patterns, shown that the flow pattern for nearly horizontal cavities, with finite aspect ratio, are convection rolls with the axis perpendicular to the longer side wall.

This is confirmed by a three-dimensional numerical and experimental study of Kirchhartz/Oertel[7] for finite boxes with aspect ratios 10:4:1 and 4:2:1. They obtain $Ra_{cr} = 1883$ for the horizontal 10:4:1 box with a linear temperature profile at the boundaries, and show that Ra_{cr} increases with decreasing aspect ratio. For small inclination angles $\alpha < 12°$ transverse rolls are shown to exist instead of longitudinal rolls, confirming the observations of Linthorst *et al.*[6]. For inclination angles from 0° to 30°, transverse rolls at the side walls already exist in the subcritical regime. For angles $\alpha > 65°$ no convection rolls are obtained. Time dependent motion sets in at $Ra \approx 6.7\, Ra_{cr}$ for the horizontal 10:4:1 box, but already at values $Ra_{osc} = 2900 \cdot \cos\alpha$ for the angle range $15° < \alpha < 60°$.

A stabilizing effect of sidewall boundaries has also been observed by Goldhirsch *et al.*[8] in a two-dimensional numerical analysis using a pseudo-spectral method. They showed that, during the build-up time, rolls already grow at the side-walls at subcritical values of Ra; the final roll number depends on Ra as well as on the symmetry of the initial distribution. Periodic time dependent motion sets in at $Ra \approx 10^5$, i.e. at a value higher than that obtained in the three dimensional analysis of Kirchhartz and Oertel.

Two dimensional finite difference calculations of transverse convection cells have been carried out by Ramanan and Korpela[9], Wright[10] and Roux *et al.*[4]. Roux *et al.* showed that no transverse rolls occurred for aspect ratios $A < 12$.

Heat transport measurements by Walden[11] for $2 < Pr < 20$ showed that three dimensional tertiary instabilities, in a horizontal layer, lead to a decrease in the Nusselt number, while the oscillatory instabilities leave the mean heat transfer coefficient nearly unchanged.

In this work, a two-dimensional simulation program has been developed in order to predict heat transfer and flow structure in cavities for a wide range of *Ra* and inclination angle α. The numerical results for high aspect ratios ($A = 20$ and $A = 40$) have been compared with both experimental data and numerical results. The code once tested has been applied to more complex geometries like double glazing and honeycomb structures.

GEOMETRY AND BOUNDARY CONDITIONS

The geometries studied are a single cavity with different aspect ratios A and inclination angles α (*Figure 1a*), a double cavity with a thin separation sheet (*Figure 1b*) and a double cavity with a separation sheet and a honeycomb structure (*Figure 1c*). *Figure 2* shows the definition of the coordinate-axis and angles in a single cavity for the simulation of transverse and longitudinal convection rolls. The boundary conditions are isothermal top and bottom plates and zero heat flux at the side walls. The case of a linear temperature profile at the edges is not studied, because boundary conditions at the side walls are shown to have little effect on the flow at high aspect ratios[12].

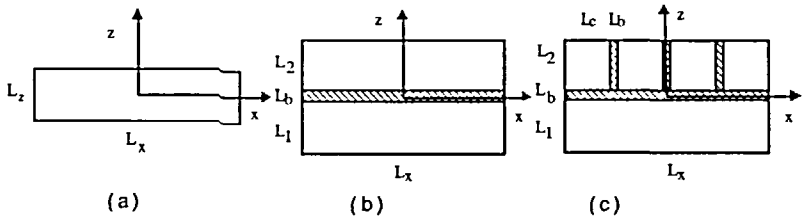

Figure 1 Geometries studied: single cavity (a), double cavity (b), double cavity with honeycomb (c)

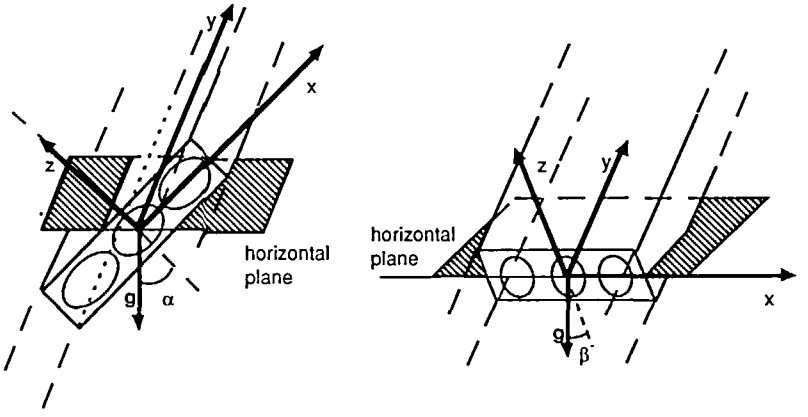

Figure 2 Definition of coordinate axis and angles in a single cavity for the simulation of transverse (a) and longitudinal (b) convection rolls

MATHEMATICAL DESCRIPTION AND NUMERICAL METHOD

The flow in the cavity is described by the Boussinesq approximation of the governing equations assuming all fluid and material properties as constant except for the density in the buoyancy terms.

A characteristic velocity is chosen balancing the convection and buoyancy terms:

$$v_0 = \frac{\nu}{L} \cdot \sqrt{\frac{Ra}{Pr}}; \tag{1}$$

If in the dimensional Navier–Stokes equations lengths are divided by L and times by $t_0 = L/v_0$, we obtain the non-dimensional equations, defining a non-dimensional temperature $T = (\theta - \theta_m)/\Delta\theta$ and pressure (with a correction representing the constant part of the gravitation force) $\tilde{p} = (p/\rho - \mathbf{r}\cdot\mathbf{g})/{v_0}^2$:

$$\dot{\mathbf{v}} + (\mathbf{v}\cdot\nabla)\mathbf{v} = \sqrt{\frac{Pr}{Ra}}\Delta\mathbf{v} - T\mathbf{g} - \nabla\tilde{p}; \tag{2}$$

$$\dot{T} + (\mathbf{v}\cdot\nabla)T = \sqrt{\frac{1}{RaPr}}\Delta T; \tag{3}$$

$$\nabla\cdot\mathbf{v} = 0; \tag{4}$$

For the description of transverse convection rolls ($g_y = 0$), i.e. for rolls with an axis orthogonal to the gravitational vector, in a cavity with infinite y-dimension all y-derivatives and the y-component of the velocity vector are zero:

$$\frac{\partial u}{\partial y} = \frac{\partial v}{\partial y} = \frac{\partial w}{\partial y} = \frac{\partial T}{\partial y} = \frac{\partial \tilde{p}}{\partial y} = v = 0; \tag{5}$$

This leads to a completely two-dimensional description of the problem:

$$\frac{\partial u}{\partial t} + u\frac{\partial u}{\partial x} + w\frac{\partial u}{\partial z} = \sqrt{\frac{Pr}{Ra}}\left(\frac{\partial^2 u}{\partial x^2} + \frac{\partial^2 u}{\partial z^2}\right) - Tg_x - \frac{\partial \tilde{p}}{\partial x}; \tag{6}$$

$$\frac{\partial w}{\partial t} + u\frac{\partial w}{\partial x} + w\frac{\partial w}{\partial z} = \sqrt{\frac{Pr}{Ra}}\left(\frac{\partial^2 w}{\partial x^2} + \frac{\partial^2 w}{\partial z^2}\right) - Tg_z - \frac{\partial \tilde{p}}{\partial z}; \tag{7}$$

$$\frac{\partial T}{\partial t} + u\frac{\partial T}{\partial x} + w\frac{\partial T}{\partial z} = \sqrt{\frac{1}{RaPr}}\left(\frac{\partial^2 T}{\partial x^2} + \frac{\partial^2 T}{\partial z^2}\right); \tag{8}$$

$$\frac{\partial u}{\partial x} + \frac{\partial w}{\partial z} = 0; \tag{9}$$

with the following boundary conditions:

$$T = 1/2 \quad \text{for} \quad z = -1/2$$

$$T = -1/2 \quad \text{for} \quad z = 1/2$$

$$\frac{\partial T}{\partial x} = 0 \quad \text{for} \quad x = \pm A/2$$

In the case of longitudinal convection rolls ($g_x = 0$) for an infinite dimension in y-direction, the y-derivatives are also zero. The y-component of the velocity vector has a finite value representing a parallel shear flow in the y-direction, which, however, as can be shown[5], neither

affects the temperature distribution, nor the x- and z-components of the velocity field. The problem can, therefore, again be reduced to a two-dimensional description becoming formally identical with the calculation for transverse cells, if we set the inclination angle α to zero and replace Ra by $Ra^* = Ra\cos\beta$, β being the inclination of the y-axis to the horizontal plane.

In order to keep a uniform mathematical formulation for the whole domain, solid structures in the cavity are accounted for by an additional term $K\mathbf{v}$ in the Navier–Stokes equation[13,14,15,16]

$$\dot{\mathbf{v}} + (\mathbf{v}\cdot\nabla)\mathbf{v} = \sqrt{\frac{Pr}{Ra}}\Delta\mathbf{v} - T\mathbf{g} - \nabla\tilde{p} + K\mathbf{v}; \tag{10}$$

and a non-dimensional thermal diffusivity $\tilde{\alpha}$ in the energy equation

$$\dot{T} + (\mathbf{v}\cdot\nabla)T = \tilde{\alpha}\sqrt{\frac{1}{RaPr}}\Delta T; \tag{11}$$

K is a very large constant ($>10^{15}$) in the solid regions, which reduces the velocity to a very small value, and elsewhere K is zero. The non-dimensional thermal diffusivity has a value $\tilde{\alpha} = \alpha/\alpha_{\text{fluid}}$.

This allows the simultaneous solution of the conduction in the solid elements and the convection-conduction in the fluid, a fact that makes the computer code easily extendable to a large variety of geometries.

The discretization of the equations follows the second-order accurate central difference scheme. It has been shown that the artificial diffusion introduced by upwinding schemes suppresses the growth of secondary convection cells[10,17]. The heat flow at the solid-fluid interface is calculated taking into account the step change in thermal conductivity:

$$q_i = \frac{T_s - T_f}{\Delta x_{si}/k_b + \Delta x_{if}/k}; \tag{12}$$

The solution of the discretized equations follows the *SIMPLEC* method described by Van Doormal and Raithby[18] using a modified strongly implicit method[19] to solve the algebraic equations.

Both transitory and pseudo-transitory calculations are carried out, the formalism being the same, but leading the fields to convergence for each time step in the first case and calculating just one iteration in the second. The maximum residual of the continuity equation, i.e. the maximum mass production/destruction in one control volume, is required to be less than $\varepsilon = 10^{-3}$ as a criterion for convergence. Where not otherwise mentioned transitory calculations have been applied.

The initial map for all calculations is $u = v = w = 0$ and $T(x, z) = -z/L_z$, i.e. a linear temperature distribution representing pure conduction.

To test the stability of the convection cells in dependence of the wavelength (number of cells) an artificial velocity field proposed by Wright[10] (Chap. 6) is applied which represents a periodic cellular flow distribution with defined wavelength $\lambda_c = 2\pi/k_c$:

$$\mathbf{v}' = \nabla \times (\psi'\cdot\hat{\mathbf{y}}); \tag{13}$$

with:

$$\psi' = \frac{\hat{\psi}}{4}\cdot[1 - (-1)^{N_c}\cdot\cos(k_c x)]\cdot[1 + \cos 2\pi z]; \tag{14}$$

The artificial velocity field $\mathbf{v}'$ is added to the original velocity field at a time, at which the base shear flow already is developed, while convection cells have not yet grown. This corresponds to a non-dimensional time of about $t = 50$ under the conditions applied in this study. The value of $\hat{\psi}$ was chosen to $\hat{\psi} = 0.2$.

The calculations have been carried out on a work station of 75 *MIPS* with a computation time of about 0.2 ms per iteration step and grid point.

RESULTS FOR A SINGLE CAVITY

Influence of the time step

The simulations of the flow in the vertical case were carried out as pseudo-transitory as well as real transitory. The results for the pseudo-transitory calculations plotted in *Figure 3a* shows

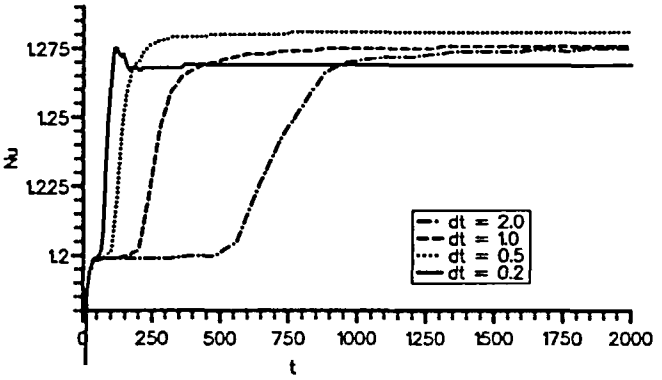

Figure 3a *Nu* vs. *t* for different time steps Δt, pseudo-transitory calculation. $Ra = 10^4$, vertical case ($\alpha = 90°$), $A = 40$, grid 200 × 24

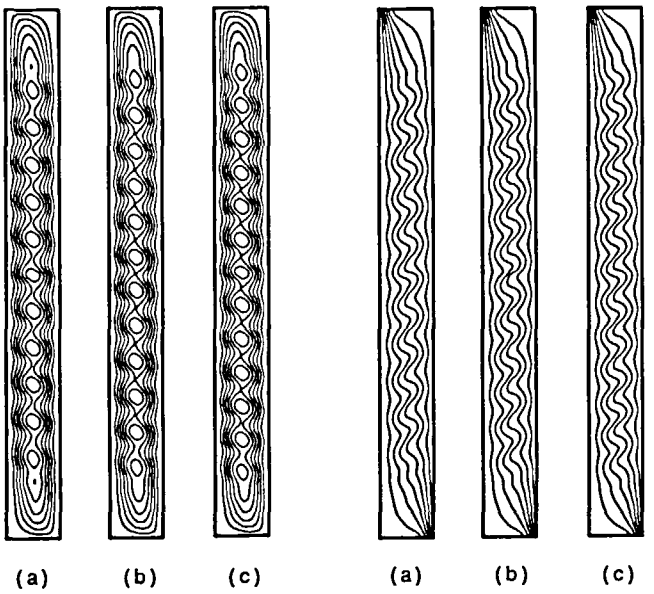

Figure 3b Streamlines (left) and isotherms (right) of the converged flow (from *Figure 3a*): $N_c = 13$, $\Delta t = 0.2$ (a); $N_c = 14$, $\Delta t = 1.0$ and $\Delta t = 2.0$ (b); $N_c = 15$, $\Delta t = 0.5$ (c). Pseudo-transitory calculation. $Ra = 10^4$, $\alpha = 90°$, $A = 40$, grid 200 × 24

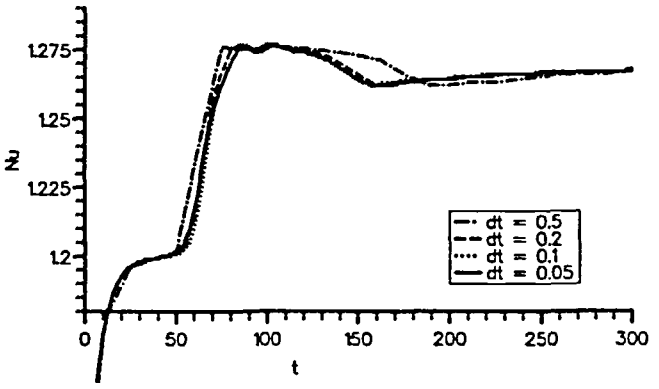

Figure 4 *Nu* vs. *t* for different time steps Δt, transitory calculation. $Ra = 10^4$, vertical case ($\alpha = 90°$), $A = 40$, grid 200 × 24

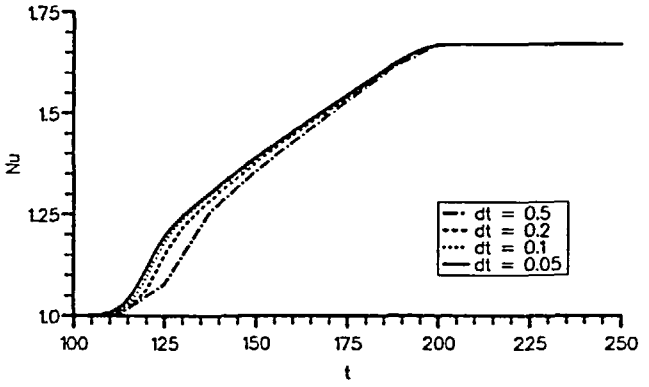

Figure 5 *Nu* vs. *t* for different time steps Δt, transitory calculation. $Ra = 10^4$, horizontal case ($\alpha = 0°$), $A = 40$, grid 200 × 24

a strong dependence on the time step of the temporal variation of the parameters as well as of the final converged structure. This indicates that the pseudo-transitory calculation is acting as a perturbation leading the development of the flow structure to one of various possible stable solutions. The streamlines and isotherms of the converged flow structure for different time-steps are plotted in *Figure 3b*. The different solutions are distinguished by the number of convection rolls, which varies from 13 to 15.

This dependence on the time step vanishes if real transitory calculation is carried out (*Figure 4*). In this case the temporal variation of flow parameters remains practically stable for a time step $\Delta t < 0.2$.

As in the vertical case, in a real transitory calculation for the horizontal cavity the dependence on the time step can be neglected for $\Delta t < 0.2$ with a grid of 200 × 24 (*Figure 5*). A pseudo-transitory calculation for this case has not been carried out.

Influence of the grid size

To elucidate the dependence of the results on the applied grid the simulation was carried out with a variety of different grid sizes (*Table 1*) for the vertical cavity. The number as well as the

Table 1 Global flow parameters of the converged solution for different grid sizes. $Ra = 10^4, \alpha = 90°, \Delta t = 0.2, t_1 = 2500$

N_x	N_z	A_{grid}	A	Nu	ψ_{max}	$\hat{\psi}_c/\psi_{max}$	N_c	λ_c	t_{CPU}
99	13	5.3	40	1.248	0.3205	0.1694	14	2.502	20.55
199	13	2.6	"	1.267	0.3163	0.2353	14	2.624	41.19
141	17	4.8	"	1.267	0.3116	0.2355	14	2.605	36.21
99	25	10.1	"	1.258	0.3013	0.1788	15	2.425	41.52
199	25	5.0	"	1.281	0.3021	0.2809	15	2.550	85.45
399	25	2.5	"	1.272	0.3077	0.2874	15	2.876	176.45
399	49	4.9	"	1.289	0.2969	0.3102	15	2.567	374.07
176	24	2.7	20	1.417	0.3082	0.2838	6	2.814	37.81
350	50	2.9	"	1.413	0.3048	0.2989	6	2.841	369.27
500	70	2.8	"	1.413	0.3042	0.3007	6	2.843	1202.26

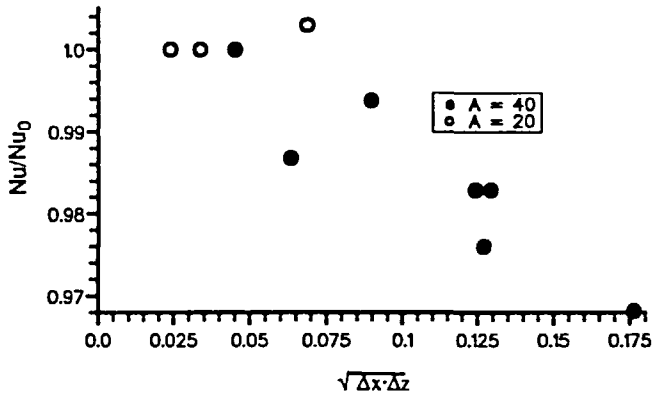

Figure 6 Nu/Nu_0 vs. $\sqrt{\Delta x \cdot \Delta z}$ for the measurements in *Table 1*. Nu_0 is the result of the measurement with the finest grid for $A = 20$ and $A = 40$ respectively

amplitude of the cells in the converged state shows a strong dependence on the grid applied indicating a convergence to an asymptotic value for the finest grid applied (45 × 70 grid points per convection cell, 500 × 70 in total). Note that, while the variation of a global parameter such as the overall-heat transfer coefficient from the finest to the coarsest grid is less than 4%, the amplitude of the periodic part of the stream function is reduced by about 46% (*Figures 6* and *7*).

A comparison of the calculations with different grids for a horizontal cavity has not yet been carried out, but the fact that the number of convection cells is higher than in the vertical case indicates that a still higher number of grid points should be applied to obtain a converged solution.

The results presented in this work for a single cavity have been calculated with a grid of 200 × 24.

Dependence on the history of the flow

As linear stability theory indicates, various stable solutions should exist for different wavelengths (i.e. numbers of convection cells) in a limited range[2]. Multistability and metastability are also observed by Kirchhartz and Oertel[7] and Goldhirsch *et al.*[8]. Therefore an attempt was made to lead the solution to different final structures by superposition of a cellular flow of different wavelengths at the moment the base flow tends to convergence while convection cells have still not grown. The wavelength and number of cells generated following (14) and the results obtained from the converged solution for a vertical box are listed in *Table 2*. The wavelength

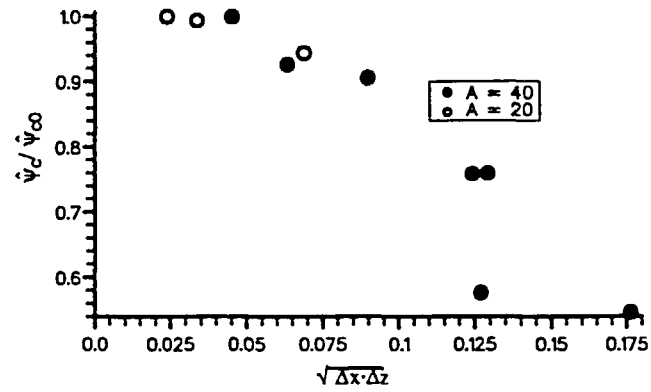

Figure 7 $\hat{\psi}_c/\hat{\psi}_{c0}$ vs. $\sqrt{\Delta x \cdot \Delta z}$ for the measurements in *Table 1*. $\hat{\psi}_{c0}$ is the result of the measurement with the finest grid for $A = 20$ and $A = 40$ respectively

Table 2 Results for the converged flow fields using a superimposed cellular flow after (14) with wavelength λ_c^s and cell number N_c^s. $Ra = 10^4$, $\alpha = 90°$, $A = 40$, $\Delta t = 0.2$, $t_1 = 1000$

N_c^s	λ_c^s	N_c	λ_c	Nu	ψ_{max}	ψ_c/ψ_{max}	
–	–	15	2.550	1.281	0.3021	0.2809	(*)
–	–	13	2.797	1.269	0.3116	0.2769	(**)
15	2.2	14	2.677	1.276	0.3079	0.2809	
14	2.4	14	2.677	1.276	0.3079	0.2817	
13	2.6	15	2.548	1.281	0.3049	0.2848	
12	2.9	14	2.677	1.276	0.3079	0.2817	

(*)$t_1 = 3000$
(**)$t_1 = 3000$, pseudo-transitory calculation with $\Delta t = 0.2$

of the converged flow is determined as the size of the central convection cell. For the value of $Ra = 10^4$ and $A = 40$ three stable states exist with 13, 14 and 15 cells, respectively. The three states can be distinguished by characteristic values of global flow parameters. The solution with $N_c = 13$ has been obtained only in a pseudo-transitory calculation and could not be reproduced by superposition of the appropriate wavelength.

The stability of the converged flow structures has been tested by superposition of a cellular flow with a wavelength of another stable solution and an amplitude of $\hat{\psi} = 0.2$. All solutions are stable to these perturbations. To obtain a change from one cell-number to another, perturbations with an amplitude $\hat{\psi} > 1$ had to be applied.

The superposition of a cellular flow in the horizontal box ($A = 40$) leads to stable solutions in the range $41 \leqslant N_c \leqslant 49$ for the number of convection cells and $1.48 < \lambda_c < 2.07$ for the cell-wavelength (*Table 3*; note that the wavelength is equal to the size of two rolls with alternate rotation). The solutions have been proved to be stable to small perturbations, as described for the vertical case.

Dependence of flow parameters on the Rayleigh-number

The plot of Nusselt versus Rayleigh number for numerical results obtained in this study for the vertical cavity ($A = 40$) compared with both experimental and other numerical results (*Figure 8*) shows a good agreement of the data in the range $6200 < Ra < 8500$, i.e. the range where stable transversal rolls exist is well represented. The onset of secondary flow is at $Ra_{cr} \approx 6200$,

Table 3 Results for the converged flow fields using a superimposed cellular flow after (14) with wavelength λ_c^s and cell number N_c^s. $Ra = 10^4$, $\alpha = 0°$, $A = 40$, $\Delta t = 0.2$, $t_1 = 1000$

N_c^s	λ_c^s	N_c	λ_c	Nu	ψ_{max}	ψ_c/ψ_{max}	
–	–	43	1.926	1.671	0.7329	0.1991	(*)
53	1.176	49	1.483	1.627	0.6979	0.1549	
51	1.224	49	1.623	1.411	0.6982	0.1470	
49	1.277	47	1.484	1.644	0.7109	0.1549	
47	1.333	45	1.686	1.663	0.7126	0.1815	
45	1.395	43	1.892	1.671	0.7254	0.1982	
41	1.463	43	1.890	1.671	0.7248	0.1983	
39	1.600	47	1.624	1.650	0.7046	0.1687	
35	1.800	43	1.826	1.671	0.7329	0.1905	
33	2.000	41	1.984	1.672	0.7455	0.1986	
29	2.200	41	2.068	1.670	0.7556	0.1946	

(*)$t_1 = 3000$

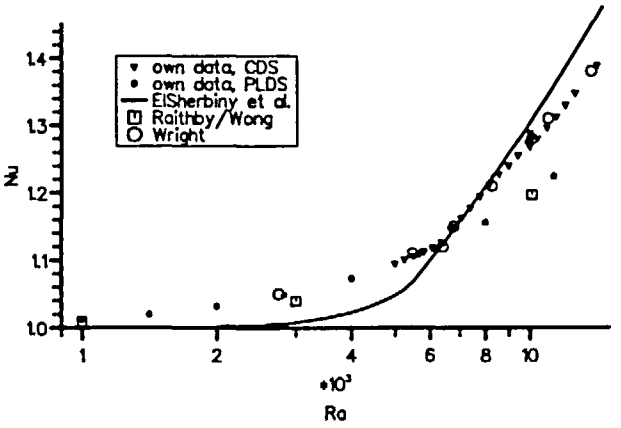

Figure 8 *Nu* vs. *Ra* for the vertical cavity from the present work in comparison with experimental results (El Sherbiny[20]) and data of other numerical studies (Raithby and Wong[12], Wright[10]). *CDS*: Central difference scheme. *PLDS*: Power law discretization scheme

a value that differs from the theoretical value 5700 for infinite boundaries due to the stabilizing effect of lateral boundaries.

Below Ra_{cr} there is a very good agreement with other numerical studies[10,12]. The numerical results differ from the experimental correlation of El Sherbiny *et al.*[20]. This is explained by the fact that the errors in the correlation equation of El Sherbiny *et al.* for the conduction regime are too big to represent the real behaviour. However, accurate experimental data in this range in order to prove this are not available.

The deviation of numerical and experimental data at $Ra > 8500$ should be due to the onset of tertiary motion. Following linear stability theory for infinite cavities[2], three-dimensional flow structures should be expected already at values of *Ra* as small as 1.06 Ra_{cr}. The good agreement of the data up to $Ra \approx 8500$ may be explained by the fact that the influence of tertiary motion like the monotone instabilities described by Chait and Korpela[2] on the overall heat transfer coefficient is small[11], and therefore experimental results are well reproduced by a two-dimensional analysis.

Figure 8 also shows that simulation results carried out with an upwinding discretization

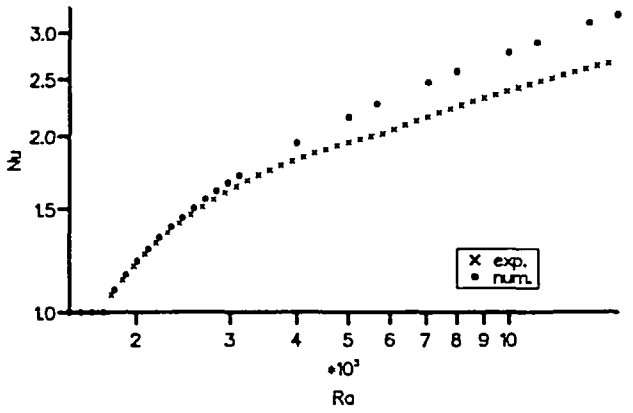

Figure 9 *Nu* vs. *Ra* for the horizontal cavity from the present work in comparison with experimental results from Hollands *et al.*[21]

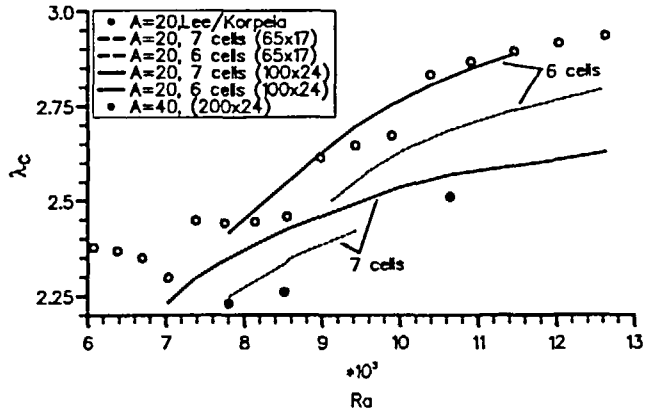

Figure 10 Cell wavelength vs. *Ra* for vertical cavities ($A = 20$ and $A = 40$) in comparison with results of Lee and Korpela[22] for $A = 20$

scheme[12,own data], which suppresses secondary cells, gives a too small heat transfer coefficient for $Ra > Ra_{cr}$.

For the horizontal cavity good agreement with the experimental results of Hollands *et al.*[21] is obtained up to $Ra \approx 2700$, indicating that, already, at $Ra = 1.4\,Ra_{cr}$ three-dimensional flow is becoming important (*Figure 9*). A base shear flow as in the vertical case does not exist due to fact that the x-component of the gravitation force is zero. The diameter of the convection cells is nearly constant throughout the whole cavity indicating that the range of influence of the walls is less than a cell-wavelength.

Figures 10 and *11* show the cell wavelength as a function of *Ra* for the vertical and the horizontal cavity, respectively. The solutions have been obtained starting from standard initial conditions without any perturbation of the flow field. The transitions between regimes with different numbers of convection cells can be clearly seen. The number of cells decreases from 15 to 11 ($A = 40$) in the plotted range of *Ra* for the vertical case, whereas it increases with increasing *Ra* from 41 to 45 ($A = 40$) for the horizontal case. For a vertical cavity with $A = 20$ the wavelength of the two stable states with 6 and 7 cells have been plotted for comparison with another

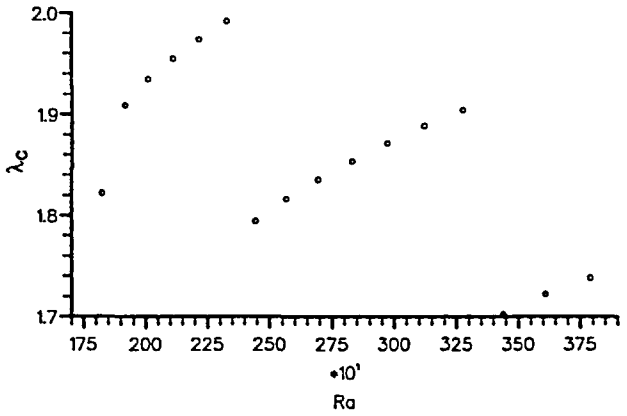

Figure 11 Cell wavelength vs. *Ra* for a horizontal cavity, $A = 40$

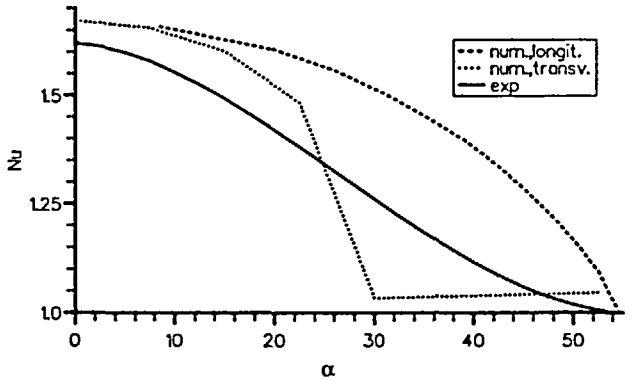

Figure 12 *Nu* vs. α for $Ra = 3000$, $A = 40$ from the present work in comparison with experimental results from Hollands *et al.*[21]

numerical study of Lee and Korpela[22]. The results of Lee and Korpela correspond to the solution with 7 convection cells and are in good coincidence with our data, if their grid (65 × 17) is applied.

Calculations for different angles of inclination

Figure 12 represents the results obtained for the overall heat transfer coefficient at different angles of inclination for both transverse and longitudinal convection rolls. It can be seen that neither of the two models gives a good description of experimental behaviour for inclined cavities. In this case three-dimensional effects should be important already at fairly supercritical values of *Ra*[4,23,24].

RESULTS FOR THE DOUBLE CAVITY

In this section results will be presented for a double cavity with a separation sheet as convection barrier (*Figure 1b*). The calculation is carried out for the following parameters:

$$\frac{L_b}{L_1 + L_2} = 0.0251; \qquad k/k_b = 0.1; \qquad A_1 = L_1/L_x = 40; \qquad \alpha_{solid}/\alpha_{fluid} = 0.005;$$

These parameters are representative for a 50 μm Teflon cover in an air filled cavity with 20 mm total plate spacing $L = L_1 + L_b + L_2$.

To obtain the *Nu* vs. *Ra* dependence of the system the calculation was carried out with time-dependent boundary conditions. A slow linear variation of *Ra* with time was obtained by raising and then decreasing the temperature difference linearly between a $\Delta\theta_{min}$ and a $\Delta\theta_{max}$. A non-dimensional heating rate defined as:

$$R = \partial(Ra_1)/\partial t; \tag{15}$$

was chosen small enough, so that over the whole region of *Ra* nearly steady state values are reached ($R = 0.2$ for the vertical cavity, $R = 0.06$ for the horizontal cavity). The fact that the growth rate of convection rolls is very small at values of *Ra*, near Ra_{cr}, leads to some kind of hysteresis in the results. The real value of Ra_{cr} lies somewhere between the values for rising and falling *Ra*.

The applied grid size was 200 × (24 + 3 + 24), 3 points of discretization for the separation sheet and 24 points for each of the two cavities in *z*-direction.

The time step was chosen as $\Delta t = 0.2$, which should be small enough to represent the real time dependence of the system following the results presented above for a single cavity.

The numerical results for the symmetrically divided horizontal cavity ($B = L_2/L_1 = 1$, $A_1 = 40$) are plotted in *Figure 13*. They have been compared with a theoretical correlation extrapolated from data of Lienhard and Catton[25,26,27] for a cavity with the parameters given above, but with infinite aspect ratio:

$$Nu = 1 + 1.704 \cdot max\left[1 - \frac{1340}{Ra_1}, 0\right]; \tag{16}$$

As an additional reference, our numerical results for a single cavity ($A = 40$) at the same heating rate and the experimental correlation of Hollands *et al.*[21] are plotted. It is demonstrated that the new boundary conditions decrease the stability of the system as pointed out by Lienhard and Catton. The critical Rayleigh number of the simulation for the double cavity is somewhat higher than the theoretically predicted value of 1340, an effect which is due to the stabilizing influence of the sidewalls in a finite-aspect ratio cavity.

Figure 14 shows the numerical results for the vertical double cavity ($B = 1$, $A_1 = 40$) in comparison with those for a single cavity ($A = 40$). Ra_{cr} for the onset of cellular motion, which

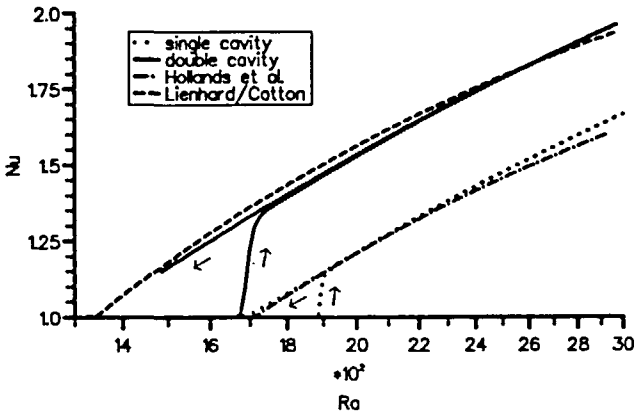

Figure 13 *Nu* vs. *Ra** for a single and a double horizontal cavity, $R = 0.2$. Single cavity: $A = 40$, $Ra^* = Ra$. Double cavity: $A_1 = 40$, $B = 1$. $Ra^* = Ra_1$. Experimental correlation for an infinite single cavity from Hollands *et al.*[21]. Theoretical correlation for an infinite double cavity after (16), based on data from Lienhard and Catton[25,26,27]

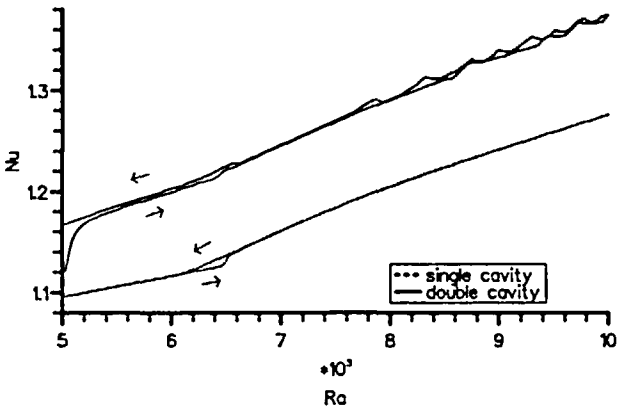

Figure 14 Nu vs. Ra^* for a single and a double vertical cavity, $R = 0.2$. Single cavity: $A = 40$, $Ra^* = Ra$. Double cavity: $A_1 = 40$, $B = 1$, $Ra^* = Ra_1$

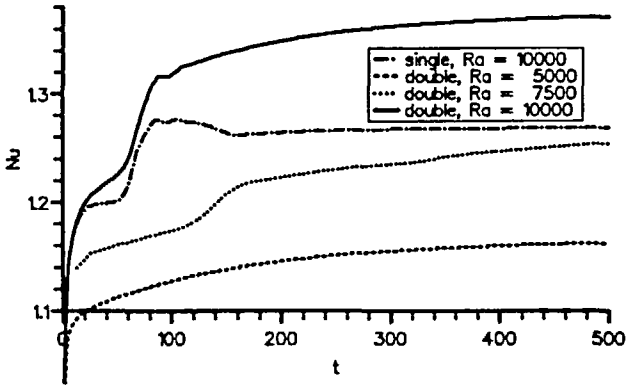

Figure 15 Nu vs. t for a vertical double cavity ($B = 1$) at $Ra_1 = 5000$, 7500, 10000 and for a single cavity at $Ra = 10000$. $\Delta t = 0.2$

can be determined as the point of a change of slope of the Nu vs. Ra curve, is nearly the same in the single and double cavity, in agreement with experimental results of Wright and Sullivan[28]. The heat transport by the base flow, however, is strongly increased. At $Ra > 7500$ the flow in the double cavity becomes unstable and shows periodic time-dependent behaviour in the two dimensional simulation with a period time $\tau_{osc} = 700$ for $Ra = 10^4$.

Figure 15 shows the build-up phase of the flow for some runs with a constant Rayleigh number. It can be seen, that the build-up time for the base flow in the double cavity is about one order of magnitude higher than that for a single cavity. The curves for the double cavity at $t = 500$ still show an increasing slope, while the corresponding curve for a single cavity reaches its asymptotic value already at about $t = 200$.

Finally, the influence of the parameter B on the heat transfer has been studied for a vertical (*Figure 16*) and a horizontal (*Figure 17*) double cavity. Only values $B \geqslant 1$ have been considered, because the solutions for $B < 1$ are the same as those for $1/B$ for reasons of symmetry[25]. For both the vertical and the horizontal cavity minimum heat transfer occurs for a symmetric division of the cavity ($B = 1$).

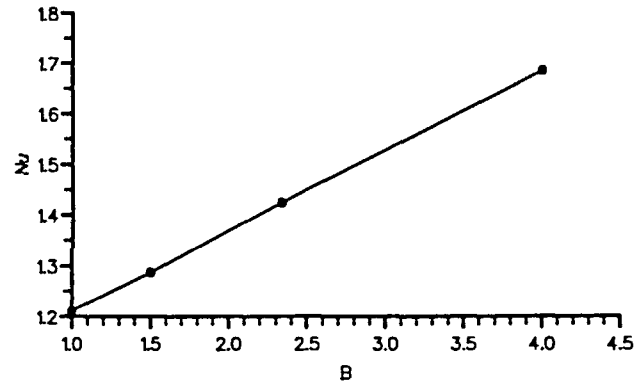

Figure 16 *Nu* vs. *B* for a vertical double cavity at $Ra = 10^5$, $A = 20$, $t_1 = 2000$, $\Delta t = 1.0$

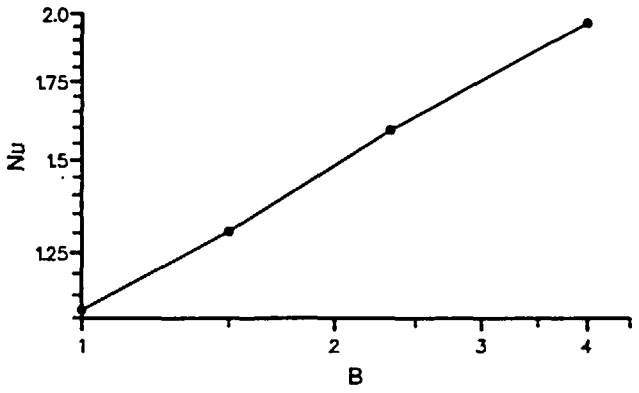

Figure 17 *Nu* vs. *B* for a horizontal double cavity at $Ra = 2.4 \cdot 10^4$, $A = 20$, $t_1 = 2000$, $\Delta t = 1.0$

RESULTS FOR THE DOUBLE CAVITY WITH HONEYCOMB

Simulations were carried out for a vertical double cavity with a honeycomb structure in one half of the domain (*Figure 1c*). The dimensions of the double cavity are the same as in the preceding section. The influence of the aspect ratio of the honeycomb cells has been studied, keeping the aspect ratio of the individual half cavity constant at $A_1 = 40$. The thickness and the thermal properties of the honeycomb material were assumed to be identical with the corresponding values for the separation sheet given in the previous section.

The number of grid points has been 24 + 3 + 24 in the z-direction and between 200 $A_c = 40$) and 500 ($A_c = 0.5$) in the x-direction.

Figure 18 shows both the isotherms and streamlines obtained for $Ra = 10^4$ at a time $t_1 = 1000$. The corresponding values of the overall heat transfer coefficient are listed in *Table 4*. It can be seen that introducing a honeycomb with cell aspect ratio $A_c > 0.5$ increases the heat transfer. This is consistent with the investigation of the aspect-ratio dependence of the heat transfer coefficient in a single cell of Raithby and Wong[12], who show that heat transfer reaches a maximum value at $A \approx 2$.

In order to study the behaviour of honeycombs with cell aspect ratios $A_c \leqslant 0.5$ calculations have been carried out for a double cavity with $A = 10$ to reduce computation time. The influence

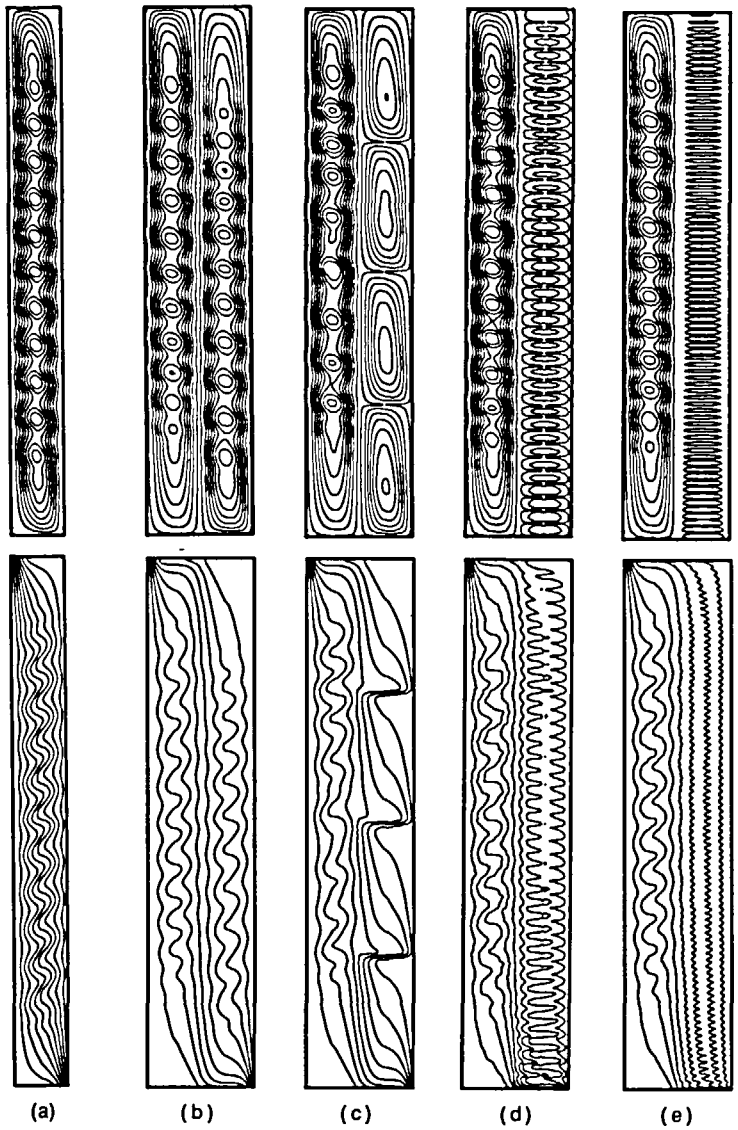

Figure 18 Streamlines (upper row) and isotherms (lower row) for a single cavity (a), a double cavity (b) and double cavities with honeycomb: $A_c = 10$ (c), $A_c = 1$ (d), $A_c = 0.5$ (e). $Ra_1 = 10^4$, $A_1 = 40$, $\alpha = 90°$

Table 4 Nu vs. A_c for a double cavity with honeycomb, $A_1 = 40$, $Ra_1 = 10^4$, $\alpha = 90°$

A_c	Nu
40	1.372
10	1.519
1	1.684
0.5	1.374

Table 5 Global flow parameters and computation time in minutes for a double cavity with honeycomb, $A = 10$, $A_c = 0.5$, $B = 1$, $Ra = 1.6 \cdot 10^5$, $\alpha = 90°$, $t_1 = 1000$, $\Delta t = 0.2$

grid	*Nu*	ψ_{max}	t_{CPU}
17 × 319	1.480	0.0771	621
25 × 439	1.444	0.0737	1268
37 × 659	1.427	0.0752	4416
49 × 879	1.422	0.0746	9103

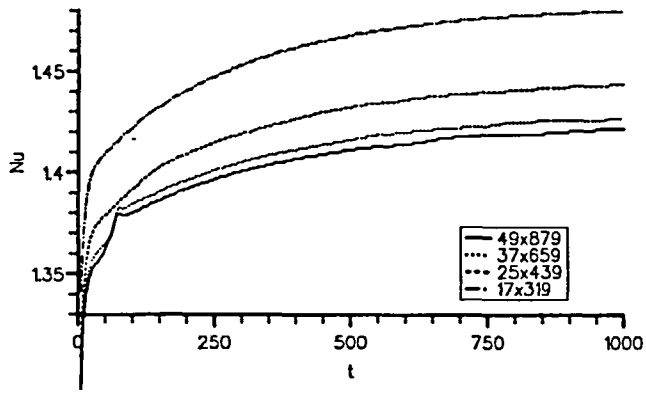

Figure 19 *Nu* vs. *t* for different grid sizes for a vertical double cavity with honeycomb. $A = 10$, $A_c = 0.5$, $B = 1$, $Ra = 1.6 \cdot 10^5$, $\Delta t = 0.2$

of the grid size has been studied for a vertical cavity with $A_c = 0.5$, $B = 1$ at $Ra = 1.6 \cdot 10^5$. The results for the heat transfer coefficient differ less than 2% for all the grids applied (*Table 5*). However, very fine grids are necessary to resolve the detailed structure of the flow. In *Figure 19* for the two finer grids an onset of secondary convection rolls can be observed at $t \approx 80$ by the sudden change of slope of the $Nu(t)$-curve while for the coarser grids this effect cannot be detected. The variation of the stream function maximum with time also shows a strong dependence on the applied grid (*Figure 20*). This indicates that still finer grids should be applied to get an asymptotic solution of the cellular part of the flow.

To keep the computation effort within a reasonable limit, in the following studies grids with 25 points in z-direction and 11 points per honeycomb cell in x-direction have been applied.

Figure 21 shows the dependence of *Nu* on the cell aspect ratio A_c. It can be seen that *Nu* first decreases with decreasing A_c due to the suppression of convection in the honeycomb, and then increases with further decreasing A_c due to the increasing influence of the conduction in the separation walls of the honeycomb.

In *Figure 22* the dependence of *Nu* on the parameter B is plotted. Due to convection suppression in the honeycomb, the minimum of heat transfer is shifted to $B > 1$.

CONCLUSIONS

- A two-dimensional simulation of natural convection in a rectangular cavity has been able to reproduce secondary flow patterns for horizontal as well as for vertical orientation for fairly supercritical values of *Ra*.

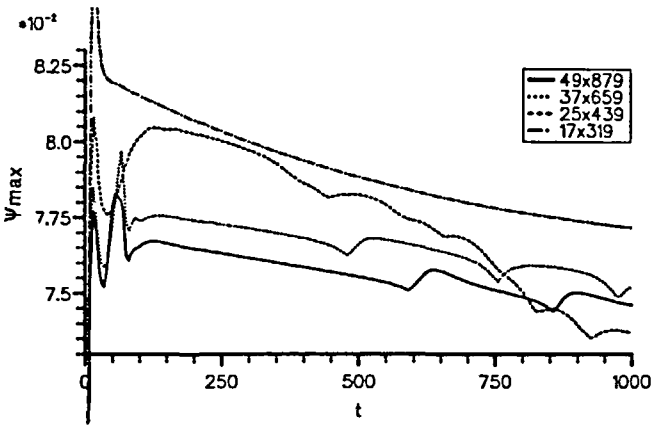

Figure 20 ψ_{max} vs. t for different grid sizes for a vertical double cavity with honeycomb. $A = 10$, $A_c = 0.5$, $B = 1$, $Ra = 1.6 \cdot 10^5$, $\Delta t = 0.2$

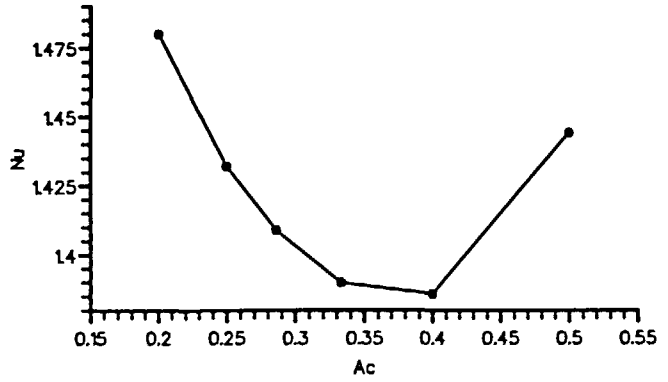

Figure 21 Nu vs. A_c for a vertical double cavity with honeycomb. $A = 10$, $B = 1$, $Ra = 1.6 \cdot 10^5$, $t_1 = 1000$, $\Delta t = 0.2$

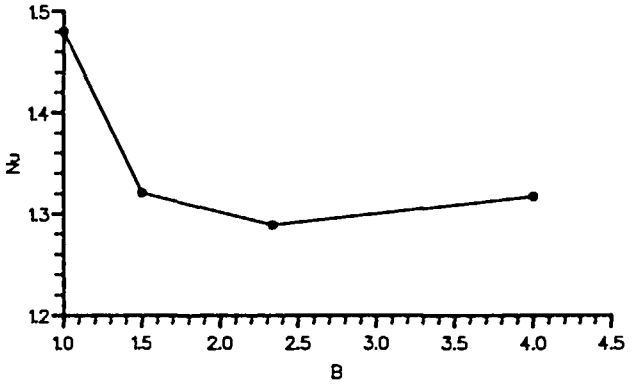

Figure 22 Nu vs. B for a vertical double cavity with honeycomb. $A = 10$, $A_c = 0.5$, $Ra = 1.6 \cdot 1^5$, $t_1 = 1000$, $\Delta t = 0.2$

- The time step and grid size required to obtain a converged solution have been shown to be $\Delta t < 0.2$ and $N_x \times N_z > 45 \times 70$ per convection cell.
- For a given supercritical Ra various stable solutions have been shown to exist with slightly different values for the heat transfer coefficient.
- Simulation fails for inclination angles which are neither nearly horizontal nor nearly vertical. In these cases three dimensional simulation will be necessary.
- The results obtained for a double cavity are in good agreement with existing theoretical and experimental investigations. The new degree of freedom of the system reduces thermal stability. Minimum heat transfer occurs for a symmetrical division of the cavity.
- Cavities with honeycomb structures have been simulated. This configuration gives a higher heat transfer than the simple double cavity for honeycomb aspect ratios $A_c > 0.5$. Convection heat transfer is reduced by a honeycomb with $A_c < 0.5$, however at small values of A_c conduction heat transfer in the separation walls of the honeycomb cells becomes important. For an optimum reduction of heat transfer an asymmetrical division of the cavity has to be foreseen, with the honeycomb structure located in the part with greater spacing.

ACKNOWLEDGEMENTS

This study has been supported by the 'Dirección General de Investigación Científica y Técnica', Project Number PB90-0606 and by the 'Departament de l'Ensenyament de la Generalitat de Catalunya'.

REFERENCES

1 Platten, J. K. and Legros, J. C. *Convection in Liquids, Chap. VI, Springer Verlag, Berlin* (1984)
2 Chait, A. and Korpela, S. A. The secondary flow and its stability for natural convection in a tall vertical enclosure, *J. Fluid Mech.*, **200**, 189–216 (1989)
3 Chen, Y. M. and Pearlstein, A. J. Stability of free-conversion flows of variable viscosity fluids in vertical and inclined slots, *J. Fluid Mech.*, **198**, 513–541 (1989)
4 Roux, B., Grondin, J.-C. and Bontoux, P. Natural convection in inclined rectangular cavities, *Proc. Press*, 423–432 (1979)
5 Clever, R. M. and Busse, F. H. Instabilities of longitudinal convection rolls in an inclined layer, *J. Fluid Mech.*, **81**, part 1, 107–127 (1977)
6 Linthorst, S. J. M., Schinke;, W. M. M. and Hoogendoorn, C. J. Natural convection flow in inclined air-filled enclosures of small and moderate aspect ratio, in *Flow Visualization II, Proc. 2. Int. Symp. Flow Visualization* (Ed. Merzkirch, W.), Sept. 9–12, Bochum, FRG (1980)
7 Kirchhartz, K. R. and Oertel, H. Jr., Three-dimensional thermal cellular convection in rectangular boxes, *J. Fluid Mech.*, **192**, 249–286 (1988)
8 Goldhirsch, I., Pelz, R. B. and Orszag, S. A. Numerical simulation of thermal convection in a two-dimensional finite box, *J. Fluid Mech.*, **199**, 1–28 (1989)
9 Ramanan, N. and Korpela, S. A. Multigrid solution of natural convection in a vertical slot, *Numerical Heat Transfer A*, **15**, 323–339 (1989)
10 Wright, J. L. *The Measurement and Computer Simulation of Heat Transfer in Glazing Systems*, Thesis, University of Waterloo, Ontario, Canada (1990)
11 Walden, R. W., Kolodner, P., Passner, A. and Surko, C. M. Heat transport by parallel-roll convection in a rectangular container, *J. Fluid Mech.*, **185**, 205–234 (1987)
12 Raithby, G. D. and Wong, H. H. Heat transfer by natural convection across vertical air layers, *Numerical Heat Transfer*, **4**, 447–457 (1981)
13 Brent, A. D., Voller, V. R. and Reid, K. J. Enthalpy-porosity technique for modelling convection-diffusion phase change: application to the melting of a pure metal, *Numerical Heat Transfer*, **13**, 297–318 (1988)
14 Voller, V. and Prakash, C. A fixed grid numerical modelling methodology for convection-diffusion mushy region phase-change problems, *Int. J. Heat and Mass Transfer*, **30**, 1709–1719 (1987)
15 Oliva, A., Costa, M. and Perez Segarra C. D. Numerical simulation of the thermal behaviour of a Trombe wall. Extended Abs. of Lectures of the Second World Cong. on Computational Mech., Stuttgart, F.R.G., pp. 685–688 (1990)
16 Costa, M., Oliva, A., Perez Segarra, C. D. and Alba, R. Numerical simulation of solid-liquid phase change phenomena, *Computer Meth. Applied Mech. Eng.*, **91**, 1123–34 (1991)

17 Drummond, J. E., Yovichin, A. J. and McKee, J. P. The effect of upwind formulations on secondary flows in a thermally driven cavity, *Proc. 3rd ASME-JSME Thermal Eng. Joint Conf.*, **1**, 47–54 (1991)
18 Van Doormaal, J. P. and Raithby, G. D. Enhancements of the SIMPLE-method for predicting incompressible fluid flows, *Num. Heat Transfer*, **7**, 147–163 (1984)
19 Schneider, G. E. and Zedan, M. A modified strongly implicit procedure for the numerical solution of field problems, *Numerical Heat Transfer*, **4**, 1–19 (1981)
20 El Sherbiny, S. M., Raithby, G. D. and Hollands, K. G. T. Heat transfer by natural convection across vertical and inclined air layers, *J. Heat Transfer*, **104**, 96–102 (1982)
21 Hollands, K. G. T., Unny, T. E., Raithby, G. D. and Konicek, L. Free convective heat transfer across inclined air layers, *J. Heat Transfer*, **98**, 189–193 (1976)
22 Lee, Y. and Korpela, S. A. Multicellular natural convection in a vertical slot, *J. Fluid Mech.*, **126**, 91–121 (1983)
23 Krishnamurti, R. Some further studies on the transition to turbulent convection, *J. Fluid Mech.*, **60**(2), 285–303 (1973)
24 Busse, F. H. Non-linear properties of thermal convection, *Rep. Prog. Phys.*, **74**, 17–35 (1974)
25 Catton, I. and Lienhard, J. H. Thermal stability of two fluid layers separated by a solid interlayer of finite thickness and thermal conductivity, *J. Heat Transfer*, **106**, 605–612 (1984)
26 Lienhard, J. H. and Catton, I. Heat transfer across a two-fluid-layer region, *J. Heat Transfer*, **108**, 198–205 (1986)
27 Lienhard, J. H. An improved approach to conductive boundary conditions for the Rayleigh-Bénard instability, *J. Heat Transfer*, **109**, 378–387 (1987)
28 Wright, J. L. and Sullivan, H. F. Glazing system U-value measurement using a guarded heater plate apparatus. Window U-value measurements symposium, ASHRAE Summer Meeting, Ottawa, *ASHRAE Transactions*, **94**, pt. 2, (1988)